The impact of Type Ia supernova explosions on helium companions in the Chandrasekhar-mass explosion scenario

Zheng-Wei Liu[1,2,3,4], R. Pakmor[5], I. R. Seitenzahl[4,6], W. Hillebrandt[4], M. Kromer[4], F. K. Röpke[6], P. Edelmann[4], S. Taubenberger[4], K. Maeda[7], B. Wang[1,2] and Z. W. Han[1,2]

zwliu@ynao.ac.cn

Received _____; accepted _____

accepted for publication in ApJ

[1]Yunnan Observatories, Chinese Academy of Sciences, Kunming 650011, P.R. China

[2]Key Laboratory for the Structure and Evolution of Celestial Objects, Chinese Academy of Sciences, Kunming 650011, P.R. China

[3]University of Chinese Academy of Sciences, Beijing 100049, P.R. China

[4]Max-Planck-Institut für Astrophysik, Karl-Schwarzschild-Str. 1, 85741 Garching, Germany

[5]Heidelberger Institut für Theoretische Studien, Schloss-Wolfsbrunnenweg 35, 69118 Heidelberg, Germany

[6]Institut für Theoretische Physik und Astrophysik, Universität Würzburg, Am Hubland, 97074 Würzburg, Germany

[7]Kavli Institute for the Physics and Mathematics of the Universe (Kavli-IPMU), Todai Institutes for Advanced Study (TODIAS), University of Tokyo, 5-1-5 Kashiwanoha, Kashiwa, Chiba 277-8583, Japan

ABSTRACT

In the version of the single-degenerate scenario of Type Ia supernovae (SNe Ia) studied here, a carbon–oxygen white dwarf explodes close to the Chandrasekhar limit after accreting material from a non-degenerate helium (He) companion star. In the present study, we employ the STELLAR GADGET code to perform three-dimensional hydrodynamical simulations of the interaction of the SN Ia ejecta with the He companion star taking into account its orbital motion and spin. It is found that only $2\% - 5\%$ of the initial companion mass are stripped off from the outer layers of He companion stars due to the SN impact. The dependence of the unbound mass (or the kick velocity) on the orbital separation can be fitted in good approximation by a power law for a given companion model. After the SN impact, the outer layers of a He donor star are significantly enriched with heavy elements from the low-expansion-velocity tail of SN Ia ejecta. The total mass of accumulated SN-ejecta material on the companion surface reaches about $\gtrsim 10^{-3}\,\mathrm{M}_{\odot}$ for different companion models. This enrichment with heavy elements provides a potential way to observationally identify the surviving companion star in SN remnants. Finally, by artificially adjusting the explosion energy of the W7 explosion model, we find that the total accumulation of SN ejecta on the companion surface is also dependent on the explosion energy with a power law relation in good approximation.

Subject headings: stars: supernovae: general - methods: numerical - binaries: close

1. INTRODUCTION

Type Ia supernovae (SNe Ia) are instrumental as distance indicators on a cosmic scale to determine the expansion history of the Universe (Riess et al. 1998; Schmidt et al. 1998; Perlmutter et al. 1999). However, neither observational nor theoretical approaches have been able to identify the nature of SN Ia progenitors and details of the explosion mechanism remain unclear (see Hillebrandt & Niemeyer 2000; Hillebrandt et al. 2013 for a review). Recently, the nearby SN 2011fe (Nugent et al. 2011; Li et al. 2011) has been used as an important test case to constrain SN Ia explosion scenarios (Röpke et al. 2012) since it can be observed in unprecedented detail. However, additional investigations are still required to put more constraints on SN Ia explosions.

It is widely believed that SNe Ia originate from thermonuclear explosions of carbon–oxygen (CO) white dwarfs (WDs) in binary systems. Depending on the nature of the companion star, the most favored progenitor models of SNe Ia are classified into two general categories, the *"single-degenerate"* (SD) scenario (Whelan & Iben 1973; Nomoto 1982) and the *"double-degenerate"* (DD) scenario (Whelan & Iben 1973; Iben & Tutukov 1984; Webbink 1984). In the DD scenario, two CO WDs spiral in and merge due to gravitational wave radiation, causing a thermonuclear explosion of the merged system. Recently, some observational and hydrodynamical studies support the viability of DD models as the progenitors of SNe Ia (see, e.g., Li et al. 2011; Nugent et al. 2011; Chomiuk et al. 2012; Horesh et al. 2012; Bloom et al. 2012; Schaefer & Pagnotta 2012; Pakmor et al. 2010, 2011, 2012b, 2013). In contrast, previous simulations suggested that the DD scenario likely leads to an accretion-induced collapse rather than a SN Ia (Nomoto & Iben 1985; Timmes et al. 1994).

In the SD scenario, a CO WD increases its mass by accreting material from a non-degenerate companion star (a slightly evolved main sequence star [MS], a red giant [RG]

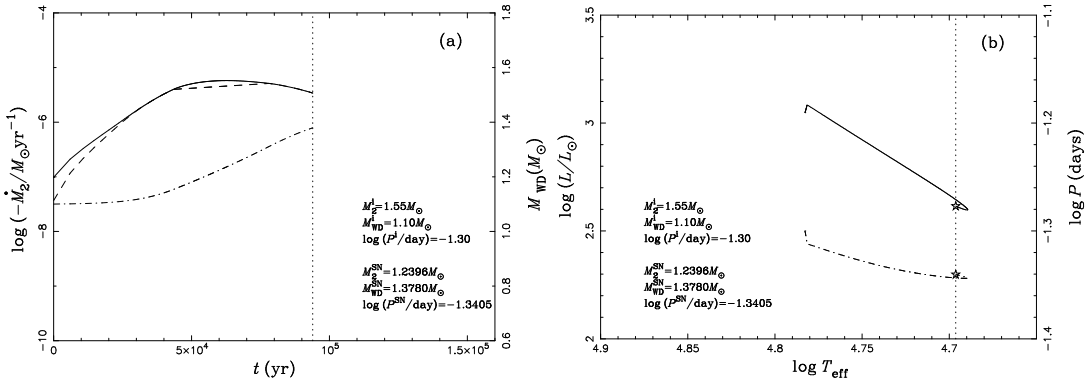

Fig. 1.— *Panel (a)*: the solid, dashed and dash-dotted curves show the mass transfer rate from the secondary, $\dot{M}_2$, the mass growth rate of the CO WD, $\dot{M}_{\rm CO}$, and the mass of the CO WD, $M_{\rm WD}$, varying with time, respectively. *Panel (b)*: the evolutionary track of the He donor star is shown as a solid curve and the evolution of orbital period is shown as a dash-dotted curve. Note that the He companion is still a MS star at the moment of the SN explosion.

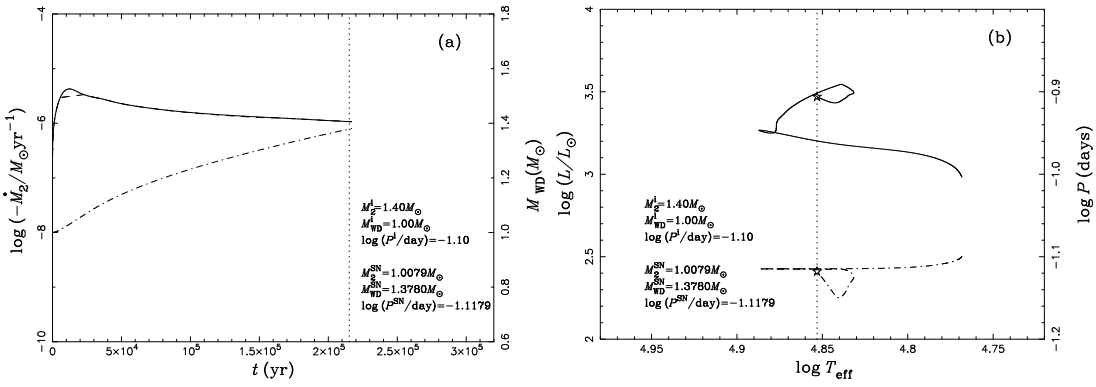

Fig. 2.— Same as Figure 1, but for the He companion star that slightly evolves to the subgiant (SG) phase at the moment of SN explosion.

or a He star [HE]) to approach the critical explosion mass (just below the Chandrasekhar limit $M_{\rm Ch} \sim 1.44\,{\rm M}_{\odot}$) to ignite a SN Ia explosion. There is evidence from observations supporting that the progenitors of some SNe Ia come from the SD channel. For example, the pre-SN circumstellar matter has been detected, and the features of the interaction of the SN explosion with circumstellar matter are seen in observations (see, e.g., Patat et al. 2007; Sternberg et al. 2011; Foley et al. 2012; Dilday et al. 2012; Shen et al. 2013). However, only a fairly narrow range of accretion rates is allowed in order to avoid nova explosions in the SD case, making it difficult to explain the observed nearby SN Ia rate(Nomoto 1982; Nomoto et al. 2007; Ruiter et al. 2009; Wang et al. 2010).

In recent years, the WD+MS and WD+RG progenitor models have been invoked to explain the observed long-delay-time ($\gtrsim 1\,{\rm Gyr}$) population of SNe Ia (see, e.g., Ruiter et al. 2009; Wang & Han 2010; Wang et al. 2010; Maoz & Badenes 2010; Maoz et al. 2010; Maoz & Mannucci 2012). Numerically, the impact of a SN Ia explosion on a MS-like or a RG companion star has been studied with hydrodynamical simulations by several authors (see, e.g., Marietta et al. 2000; Pakmor et al. 2008; Pan et al. 2010, 2012; Liu et al. 2012, 2013). They found that ~ 0.03–$0.15\,{\rm M}_{\odot}$ H-rich material can be stripped off from the surface of MS companion stars. For RG companions it is believed that the entire envelope is stripped off by the SN impact. This high stripped mass is far larger than the most stringent upper limit of $0.01\,M_{\odot}$ which Leonard (2007) derived from the non-detection of $\rm H_{\alpha}$ emission in late time spectra (see also Shappee et al. 2013). So far, in fact, no direct observation shows the signature of stripped H-rich material, which seriously challenges SD progenitor scenario.

In the spin-up/spin-down model for SNe Ia[1], however, the donor star might shrink

[1]In the SD scenario, a WD accretes and retains companion matter that carries angular momentum. As a consequence the WD spins with a short period which leads to an increase

significantly because it exhausts the H-rich envelope before the explosion sets in after a spin-down phase of $> 10^5$ yrs. Thus, the donor star could be too dim to detect by the time of explosion and much smaller than its Roche lobe (see Di Stefano et al. 2011; Justham 2011). This may reduce the possibility of the detection of H lines in SN Ia nebular spectra and possibly provides an explanation for the apparent lack of a 'left-over' star in LMC SN remnant SNR 0609 − 67.5 (Di Stefano & Kilic 2012).

In the so-called WD+HE channel a CO WD accretes material from a He companion star. This may initiate a thermonuclear explosion of the WD. At present, two possible explosion models are frequently discussed: the sub-$M_{\rm Ch}$ scenario (Woosley & Weaver 1994; Fink et al. 2007, 2010; Woosley & Kasen 2011) and the $M_{\rm Ch}$ scenario (Wang et al. 2009b,a). In this paper, however, we only focus on the WD+HE $M_{\rm Ch}$ model. With a binary population synthesis (BPS) approach, Wang et al. (2009b) (hereafter WMCH09) comprehensively and systematically investigated WD+HE $M_{\rm Ch}$ systems and showed that this channel can explain SNe Ia with short-delay times ($\lesssim 10^8$ yrs), which is consistent with recent observational implications of young populations of SN Ia progenitors (Wang et al. 2009b,a).

Recently, Pan et al. (2010, 2012) investigated the impact of SN Ia ejecta on a He companion star including the rotation of the He star by using Eulerian hydrodynamics simulations with the FLASH code. They found the He companion star could be contaminated by the SN Ia ejecta in its outer envelope after the impact, and the nickel contamination is $\sim 10^{-4}\,M_\odot$ (Pan et al. 2010, 2012). This might help to identify surviving companion stars in the remnants of historical SNe Ia even a long time after the explosion.

---

of the critical explosion mass. If the critical mass is higher than the actual mass of the WD, the SN explosion can only occur after the WD increases the spin period with a specific spin-down timescale (see Di Stefano et al. 2011; Justham 2011).

Table 1: Results of SPH impact simulations.

Model[a]	$v_{\rm orb}$	$v_{\rm spin}$	R_2	A	$M_{\rm unbound}$	$v_{\rm kick}$	$\delta M_{\rm tot}$[b]	$\delta M_{\rm Fe}$[b]	$\delta M_{\rm Ni}$[b]	$M_{\rm Ni}/M_{\rm He}$[c]	$M_{\rm Fe}/M_{\rm He}$[c]
	($\rm km\,s^{-1}$)		(10^{10} cm)		($\rm M_\odot$)	($\rm km\,s^{-1}$)	($10^{-3}\,\rm M_\odot$)			(10^{-3})	(10^{-3})
W7_He01	-	-	1.91	5.16	0.027	66.39	5.22	3.52	1.59	1.63	3.62
W7_He02	-	-	2.48	7.04	0.056	58.75	3.12	2.16	0.88	3.54	8.72
W7_He01_r	432	301	1.91	5.16	0.028	66.94	5.37	3.49	1.81	1.85	3.57
W7_He02_r	387	237	2.48	7.04	0.057	59.74	3.14	2.02	0.96	3.86	8.11
W708_He01_r	432	301	1.91	5.16	0.019	39.93	12.06	7.49	4.44	4.52	7.61
W710_He01_r	432	301	1.91	5.16	0.024	52.53	8.30	5.29	2.91	2.97	5.39
W714_He01_r	432	301	1.91	5.16	0.033	75.89	3.97	2.57	1.38	1.38	2.64
W716_He01_r	432	301	1.91	5.16	0.037	86.08	2.71	1.80	0.87	0.90	1.86

Note. —

[a] "W7" corresponds to the W7 explosion model (Nomoto et al. 1984; Maeda et al. 2010). "W708", "W710", "W714" and "W716" present W7-like models that are produced by adjusting the original W7 model with different explosion energies ($0.8, 1.0, 1.4$ and 1.6×10^{51} erg). Note that all parameters but the SN energy are kept constant with the values of the original model (see also Pakmor et al. 2008). "He01" and "He02" are two He companion models. "r" means that the orbital motion and spin of the He companion are included.

[b] $\delta M_{\rm tot}$, $\delta M_{\rm Fe}$ and $\delta M_{\rm Ni}$ are the total contamination, the accreted Fe and Ni mass at the end of the simulations ($\gtrsim 2000$ s after the explosion), respectively.

[c] The ratio of bound Ni and Fe masses (without decay) to the He masses of a surviving star. Please note that the initial metallicity of the He star is not included.

In their simulations, however, the He star companion models were constructed by artificially adopting a constant mass-loss rate to mimic the detailed binary evolutionary models of WMCH09.

In this work, we update the He companion star models with one-dimensional (1D) consistent binary evolution calculations. Then, we perform hydrodynamics simulations of the interaction of SN Ia ejecta with He companion stars. To this end we use the three-dimensional (3D) smoothed particle hydrodynamics (SPH) code Stellar GADGET. In Section 2, the code and the initial setup are introduced. The results of the SPH impact simulations are discussed on the basis of two consistent He companion star models in Section 3. All numerical results are presented in Section 4. Finally, we summarize our results and conclude in Section 5.

2. CODES AND INITIAL MODELS

We use Eggleton's stellar evolution code (Eggleton 1971, 1972, 1973) to follow the detailed binary evolution of WD+HE progenitor systems. The Roche lobe overflow (RLOF) is treated in the code as described by Han & Podsiadlowski (2004). In this work, we only focus on $M_{\rm Ch}$ explosions of accreting WDs. The influence of rotation on the He-accreting WDs is not considered in the stellar evolution calculations. Our basic input physics and initial setup in the code are the same as those in WMCH09. The He companion star is evolved without enhanced mixing, i.e., the convective overshooting parameter, $\delta_{\rm ov} = 0$ (see Dewi et al. 2002). Initial He star models are set up with a He abundance of $\rm Y = 0.98$ and a metallicity of $\rm Z = 0.02$. In addition, orbital angular momentum loss due to gravitational wave radiation (GWR) is included by adopting a standard formula presented by Landau & Lifshitz (1971):

$$\frac{\mathrm{d}\ \ln J_{\rm GR}}{\mathrm{d}t} = -\frac{32G^3}{5c^5}\frac{M_{\rm WD}M_2(M_{\rm WD}+M_2)}{A^4}, \tag{1}$$

where $G, c, M_{\rm WD}$ and M_2 are the gravitational constant, vacuum speed-of-light, mass of the accreting WD and mass of the He companion star, respectively.

We start to trace the binary evolution when the WD+HE binary system is formed. The mass transfer occurs through RLOF once the He donor star fills its Roche lobe. Here, we do not solve the stellar structure equations for the WD star when the structures of the companion stars are constructed. Instead, we used the optically thick wind model of Hachisu et al. (1996, 1999) and adopt the prescription of Kato & Hachisu (2004) for the mass accumulation efficiency of He-shell flashes onto the WD primary. If the mass transfer rate, $\dot{M}_2$, is above a critical value, $\dot{M}_{\rm cr}$, we assume that He burns steadily on the surface of the WD and that the He-rich material is converted into carbon and oxygen at the rate $\dot{M}_{\rm cr}$, while the unprocessed matter is assumed to be lost from the system as an optically thick wind at a mass-loss rate $\dot{M}_{\rm wind} = \left|\dot{M}_2\right| - \dot{M}_{\rm cr}$. The critical mass-accretion rate is (Nomoto 1982)

$$\dot{M}_{\rm cr} = 7.2\times10^{-6}(M_{\rm WD}/{\rm M}_\odot - 0.6)\ {\rm M}_\odot\,{\rm yr}^{-1}, \tag{2}$$

When $\left|\dot{M}_2\right|$ is smaller than $\dot{M}_{\rm cr}$, the following assumptions have been adopted:

1. If $\dot{M}_{\rm st} \leqslant |\dot{M}_2| \leqslant \dot{M}_{\rm cr}$, it is assumed that there is no mass loss and that He-shell burning is steady, where $\dot{M}_{\rm st}$ is the minimum accretion-rate of stable He-shell burning from Kato & Hachisu (2004).

2. If $\dot{M}_{\rm low} \leqslant \left|\dot{M}_2\right| < \dot{M}_{\rm st}$, He-shell burning is unstable, He-shell flashes occur and a part of the envelope mass is assumed to be blown off from the surface of the WD. Here,

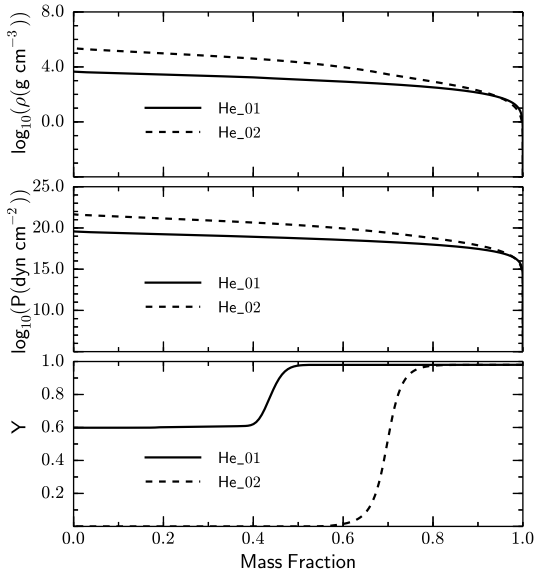

Fig. 3.— Profiles of the density ρ, pressure P, and helium abundance Y as a function of enclosed mass m at the moment of the SN explosion for the He01 model (solid lines) and He02 model (dashed lines).

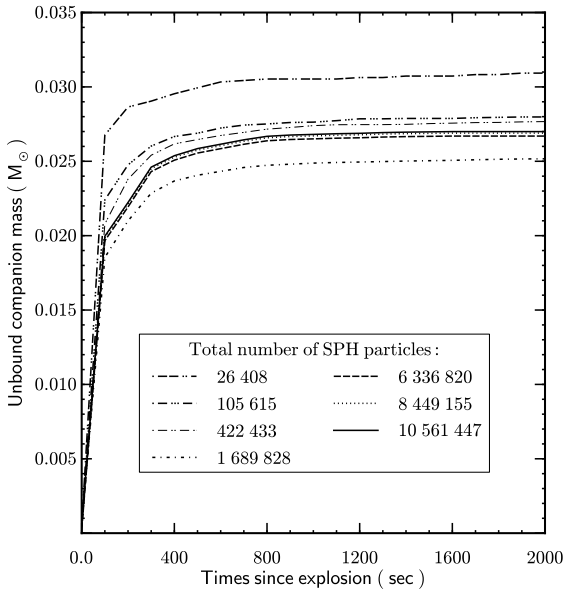

Fig. 4.— Unbound companion mass vs. time since explosion in W7_He01 model for different resolutions ($\sim 10^4 - 10^7$ SPH particles in the simulations).

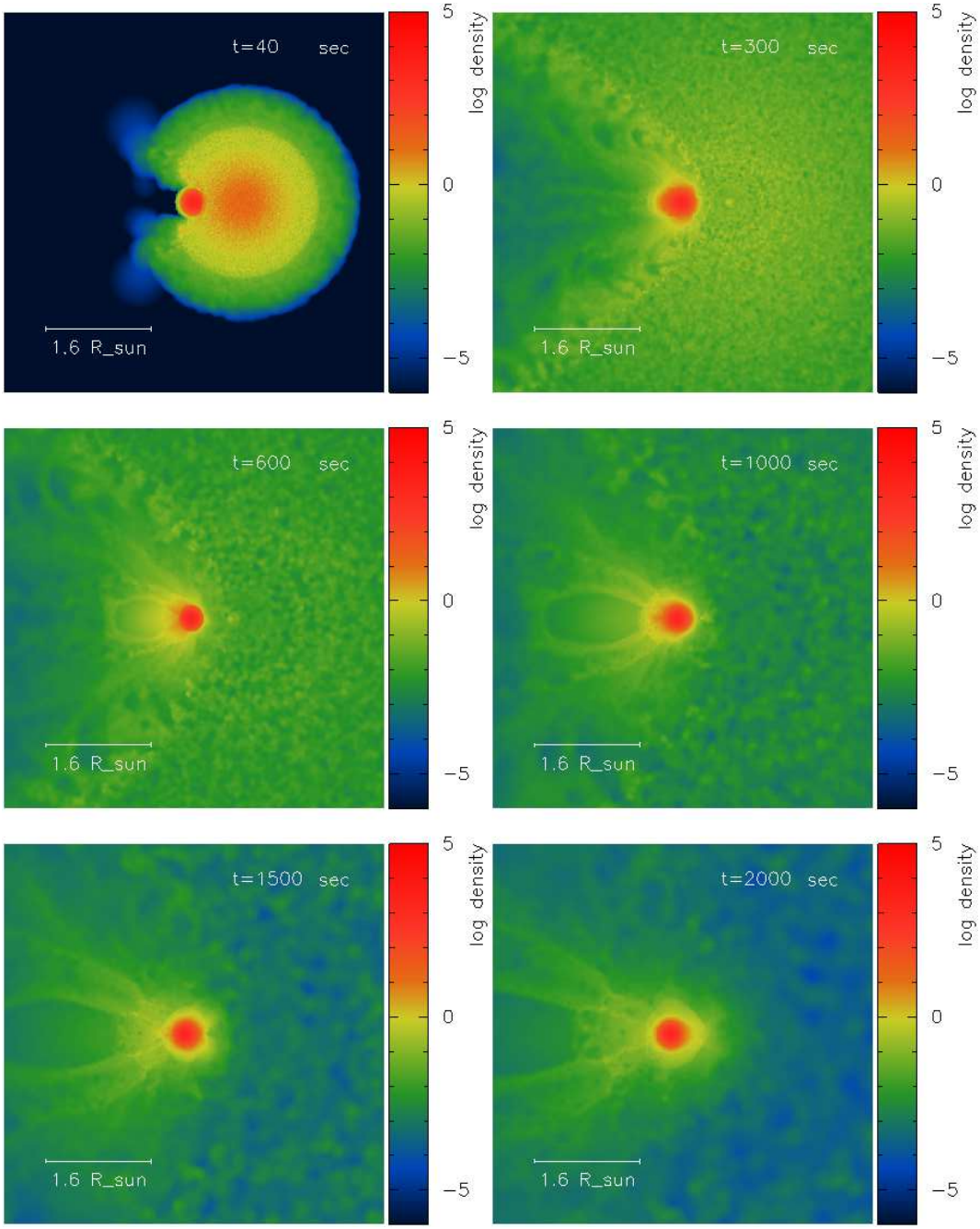

Fig. 5.— Temporal evolution of the density structure of SN and companion material in impact simulations with W7_He01 model. The color scale indicates the logarithm to base 10 of density in $\mathrm{g\,cm^{-3}}$. The plots are made using the freely available SPLASH code (Price 2007).

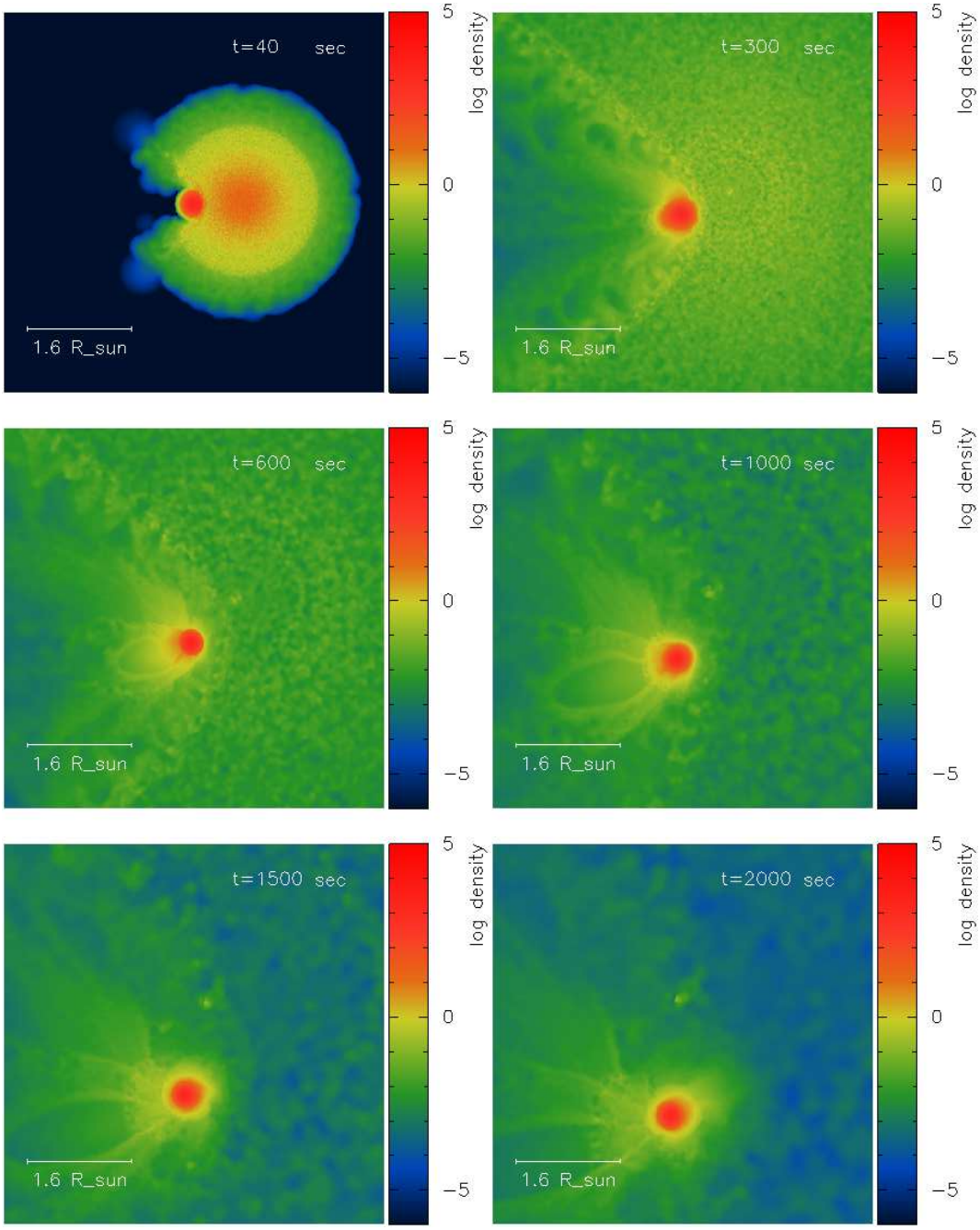

Fig. 6.— Same as Figure 5, but for the W7_He01_r model (which includes the orbital motion and spin of He companion). The color scale indicates the logarithm to base 10 of density in $\mathrm{g\,cm^{-3}}$. The plots are made using the freely available SPLASH code (Price 2007)

$\dot{M}_{\rm low} = 4.0 \times 10^{-8}\,{\rm M}_\odot\,{\rm yr}^{-1}$ is the minimum accretion-rate of weak He-shell flashes (Woosley et al. 1986).

3. If $\left|\dot{M}_2\right| < \dot{M}_{\rm low}$, He-shell flashes are so strong that no mass can be accumulated by the WD (i.e., the mass-growth rate of the WD is zero).

Finally, two He companion star models based on detailed binary evolution calculations are chosen as representative examples to perform SPH impact simulations. They are named with "He01" and "He02". The typical binary evolution calculations of these two models are shown in Figure 1 (He01 model) and Figure 2 (He02 model). In the He01 model (companion mass $M_2^{\rm SN} = 1.2396\,{\rm M}_\odot$, orbital separation $A = 5.16 \times 10^{10}\,{\rm cm}$, companion radius $R_2 = 1.91 \times 10^{10}\,{\rm cm}$) the companion star remains to be a He MS star (central He burning), whereas in the He02 model ($M_2^{\rm SN} = 1.0079\,{\rm M}_\odot$, $A = 7.04 \times 10^{10}\,{\rm cm}$, $R_2 = 2.48 \times 10^{10}\,{\rm cm}$) it has evolved slightly into the subgiant phase (central He exhausted) at the onset of the SN Ia explosion. The structure profiles of two companion stars (the He01 and He02 model) at the moment of SN Ia explosion are shown in Figure 3.

The hydrodynamical simulations of the impact of SN Ia ejecta on the He companion star are performed with the 3D SPH code Stellar GADGET (Pakmor et al. 2012a; Springel 2005). In our simulation, we use the same method as Liu et al. (2012) to map the 1D profiles of density and internal energy of a 1D companion star model to a particle distribution suitable for the SPH code. To reduce numerical noise introduced by the mapping, the SPH model of each companion star is relaxed for several dynamical timescales ($1.0 \times 10^4\,{\rm s}$) before we start the actual impact simulations. If the relaxation succeeds, the velocities of the particles stay close to zero. Otherwise, we reject the SPH model, and repeat the relaxation after adjusting the relaxation parameters (Pakmor et al. 2012a).

The SN explosion is represented by the W7 model of Nomoto et al. (1984); Maeda et al. (2010). This model has been shown to provide a good fit to the observational light curves

of SNe Ia (Lentz et al. 2001). Its total explosion energy is 1.23×10^{51} erg, the average velocity of the ejecta $10^4\,\mathrm{km\,s^{-1}}$. Based on the 1D W7 model of Nomoto et al. (1984), SPH particles are placed randomly in shells to reproduce the mass (density) profile and gain the radial velocities they should have at their positions (all particles have the same mass). The composition of a particle is then set to the values of the initial 1D model at a radius equal to the radial coordinate of the particle. In our hydrodynamical simulations, the impact of the SN Ia ejecta on the companion is simulated for $\geq 2000\,\mathrm{s}$ taking into account the orbital motion and spin of the He companion star. Here, we assume that the rotation of the companion star is in phase-locked to its orbital motion. Moreover, we set the $x-y$ plane as the orbital plane of the binary system with an assumption of a circular orbit. The $z-$axis is chosen as the rotation axes, and, when the spin of the companion star is included, the positive $z-$axis is the direction of the angular momentum.

3. SIMULATIONS

3.1. Resolution Test

We use the W7_He01 model (see Table 1) as a typical case to perform a convergence test to check the sensitivity of unbound mass to different resolutions. By adopting a fixed orbital separation ($A = 5.16 \times 10^{10}\,\mathrm{cm}$), the resolutions are set up with different number of total SPH particles ranging from 2.64×10^4 to 1.05×10^7. The unbound companion mass caused by the SN impact as a function of time since explosion for each resolution is plotted in Figure 4. The unbound mass is calculated by summing up the total mass of all particles that originally belonged to the He companion star but are unbound after the impact. In order to determine whether or not a particle is bound to the star, we calculated the total energy of each particle at each time step, $E_{\mathrm{tot}} = E_{\mathrm{kin}} + E_{\mathrm{pot}} + E_{\mathrm{in}}$, where E_{kin}, E_{pot} and E_{in} are the kinetic energy (positive), the potential energy (negative) and the internal energy

(positive), respectively. If $E_{\rm tot} > 0$, the particle is unbound. Note that the center-of-mass motion of the star is subtracted when calculating the kinetic energy for each particle.

Figure 4 shows the amount of unbound companion mass asymptotically approaches a final value at late times. For the simulations that span a range of 400 in mass resolution from the lowest to the highest mass resolution the stripped mass measured in those simulations deviates less than 25% from the highest resolution run. Therefore, our results are clearly sufficiently well converged to allow a meaningful comparison to observational constraints, which are still uncertain by a factor of a few (Leonard 2007). Note that we also carried out the convergence test for the amount of SN ejecta that are captured by the companion star after the SN explosion (for different resolutions of $\sim 2.64 \times 10^4$–1.06×10^7, the captured SN ejecta masses at the end of simulations are $0.0064, 0.0067, 0.0075, 0.0072, 0.0060, 0.0059,$ and $0.0053\,{\rm M}_\odot$). We found that it is also sufficiently well converged. Therefore, we chose the level of 5 million SPH particles to represent the He companion stars (which corresponds to the total particles of $\sim 10^7$) in all following impact simulations.

3.2. Typical Evolution after the SN Ia Explosion

Figure 5 illustrates the temporal density evolution of the SN ejecta and companion material of our hydrodynamics simulations for the W7_He01 model. Before the SN explosion, the He companion star is filling its Roche lobe. The WD explodes as a SN Ia on the right side of the companion star. The SN ejecta expand freely for a while before hitting the surface of the donor star which faces towards the explosion (see first snapshot). A shock wave develops while the He-rich material is stripped-off from the companion star. This shock wave propagates through the whole companion star and strips off additional material from the far side of the companion. As the SN ejecta flow around the companion star, a cone-shaped hole with an opening angle with respect to the $x-$axis of $\sim$35° forms in

the SN ejecta (see Figure 5). At the end of the hydrodynamics simulations, about 0.027 $M_{\odot}$ of He-rich material is stripped off due to the SN impact. The companion star survives the explosion, but it is completely out of thermal equilibrium and dramatically expanding due to the SN heating. Compared with our previous work on WD+MS models (Liu et al. 2012), this effect is more significant since He companion stars have higher orbital velocities.

Figure 6 shows how the orbital motion and the spin of the He companion star affect the density structures of the SN ejecta and the companion star. In this work, the hydrodynamics simulations are carried out for He01 and He02 models (see Table 1) by including their orbital and spin velocities. All simulated results are shown in Table 1. Note that "W7" means the W7 explosion model, the letter "r" indicates that the orbital motion and spin of the companion star are included into the simulations. It is evident that the additional unbound mass and kick velocity caused by including the orbital motion and spin is very small (see Table 1), the difference being within 2% compared to non-rotating models.

3.3. Parameter Study

At the end of the simulations, only 0.03–0.06 $M_{\odot}$ of He-rich companion material is found to be stripped off in impact simulations of two different He companion models. Meanwhile, the companion star receives a small kick velocity of ∼58–67 km s^{-1} at the end of the simulations. In order to explore the sensitivity of the numerical results on the orbital separation, we run several simulations by artificially adjusting the binary separations of the "W7_He01" and "W7_He02" models. All other parameters are kept constant at the values of the original model. Figure 7 shows the unbound mass and kick velocity as functions of the binary orbital separations, which is consistent with other similar impact hydrodynamics simulations (Pan et al. 2010, 2012). For a given companion model, the unbound mass decreases as the separation becomes larger. It is found that this relation follows a power

law in good approximation, and can be fitted as (see Figure 7a):

$$M_{\rm unbound} = C_1 \left(\frac{A}{R_2}\right)^{-\alpha} \quad {\rm M}_\odot, \tag{3}$$

where A is the binary separation, R_2 is the radius of the He companion star at the onset of the SN explosion, C_1 is a constant and α is the power-law index. All fitting parameters are listed in Table 2. Moreover, the dependence of the kick velocity, $v_{\rm kick}$, on A/R_2 can also be fitted by a power law (see Figure 7b):

$$v_{\rm kick} = C_2 \left(\frac{A}{R_2}\right)^{-\beta} \quad {\rm km\,s^{-1}}, \tag{4}$$

where C_2 is a constant and β is the power-law index (see Table 2).

The different companion star models lead to different fitting parameters. This indicates that the companion structure plays an important role in our impact simulations also. For example, the binding energy of the companion envelope would affect it. In order to compare with other hydrodynamics simulations, the results of the He-WDc model of Pan et al. (2010) ($M_2 = 1.007\,M_\odot$, $A = 4.0 \times 10^{10}\,{\rm cm}$ and $R_2 = 1.35 \times 10^{10}\,{\rm cm}$ at the moment

Table 2: Fitting parameters for equation (3) and (4)

	Fitting parameters			
Model	C_1	α	C_2	β
W7_He01	0.54	2.96	689	2.37
W7_He02	0.34	1.75	247	1.38

of the SN explosion)[2] is chosen to compare with our W7_He02 model ($M_2 = 1.007\,M_\odot$, $A = 7.04 \times 10^{10}\,\mathrm{cm}$ and $R_2 = 2.48 \times 10^{10}\,\mathrm{cm}$). The unbound mass and kick velocity in their He-WDc model are more sensitive to the orbital separation than in our W7_He02 model (see Figure 7). The difference might be caused by different companion structures. In their 1D calculations, the mass-transfer from the He companion star was modeled by adopting a constant mass-loss rate to mimic the work of WMCH09 (see Pan et al. 2010). The orbital separation at the moment of the SN explosion was calculated using the formulation of Eggleton (1983). In our consistent binary calculations, however, we trace the details of the binary evolution by treating the mass-transfer as RLOF, which also fixes the separation of the binary system at this moment.

Based on the distribution of the parameter A/R_2 in population synthesis calculations of WMCH09 (see Figure 8a), we simply calculate the unbound masses due to the SN impact by using equation (3). The derived distribution for the unbound mass is shown in Figure 8b, where the peak unbound mass ranges from $0.02\,\mathrm{M}_\odot$ to $0.05\,\mathrm{M}_\odot$.[3] The difference between the W7_He02 and He-WDc model, again indicates that the details of the companion structures are important for the interaction of SN Ia ejecta with the companion star.

---

[2]The He-WDc model of Pan et al. (2010), was set up to mimic a system obtained from detailed binary evolution in WMCH09. This corresponds to our W7_He02 model.

[3]Note that we use the same power-law relation for different A/R_2 (different companion models) to predict the unbound masses. However, it is found that different companion models would lead to different fitting parameters in SPH simulations (see Figure 7).

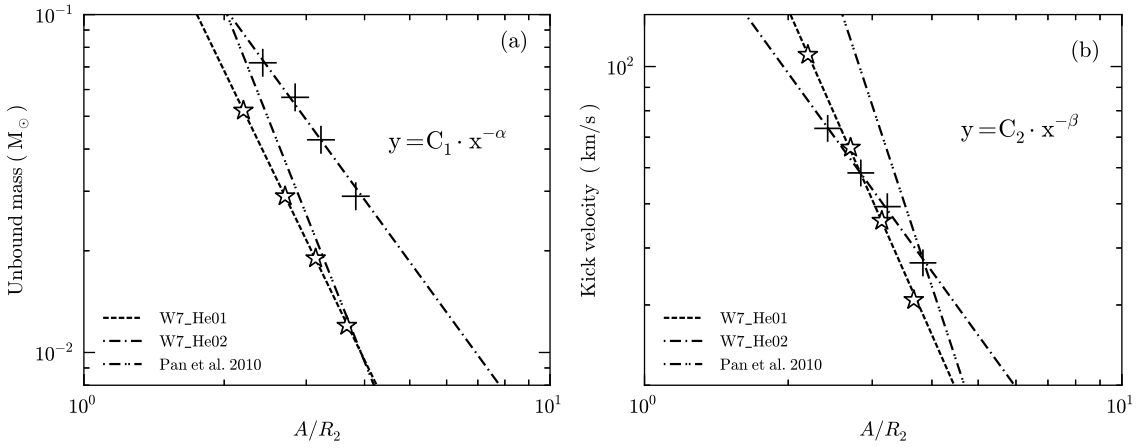

Fig. 7.— Mass stripped-off from the companion (a) and kick velocity (b) as functions of the ratio of the orbital separation to the radius of the companion, A/R_2, for a given He companion model. The star and corss symbols represent the results of our impact simulations for the He01 model and He02 model. Lines show fitted power-law relations based on the numerical simulation results.

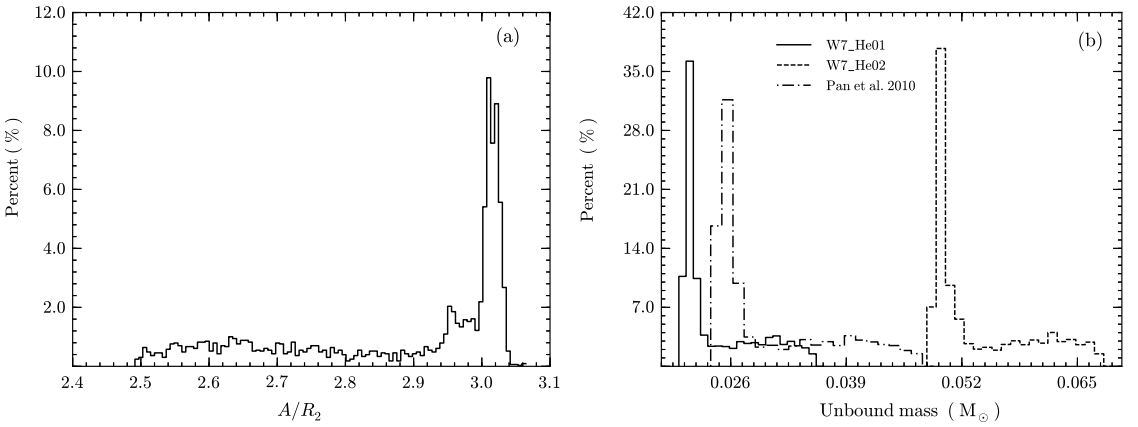

Fig. 8.— *Panel (a)*: Distribution of the parameter, A/R_2, based on the population synthesis results for WD+HE models (Wang et al. 2009a). *Panel (b)*: The corresponding distribution of unbound mass due to the SN impact. The unbound mass is calculated by using the power law relation of equation (3).

4. DISCUSSION

4.1. Effect of Ablation

After the SN explosion, the unbound He-rich material from the companion star may result from two mechanisms: ablation (SN heating) and stripping (momentum transfer). Pan et al. (2012) found that the stripped-to-ablated mass ratio for the He-WD scenario was about 0.5–0.8 in their impact simulations with the FLASH code. They argued that previous analytical or semi-analytical work underestimated the unbound mass due to the neglect of ablation.

To obtain the stripped-to-ablated mass ratio, we compare the internal energy of a companion particle to its kinetic energy once it becomes unbound. If the internal energy is larger (or smaller) than the kinetic energy, we think the particle is ablated (or stripped). We then use the SPH particle's ID to trace all these ablated (or stripped) particles to the end of the simulations (2000 s after the impact). The total ablated (stripped) mass is calculated by summing the particles that are ablated (stripped) and still unbound at the end of the simulations. Finally, we obtain a stripped-to-ablated mass ratio of ~ 0.5, which is consistent with the results of Pan et al. (2012).

Moreover, we calculate the amount of unbound mass by summing the total mass of all unbound particles for each time step, where we do include internal energy of the particle (i.e., $E_{\rm tot} = E_{\rm kin} + E_{\rm pot} + E_{\rm in}$, which corresponds to the dashed line in Figure 9) or do not (i.e., $E_{\rm tot} = E_{\rm kin} + E_{\rm pot}$, which corresponds to the solid line in Figure 9). The companion particles are ablated and stripped and become unbound in early stage of the explosion. As times goes by, the internal energy of the particle converts into their kinetic energy. Moreover, some ablated and stripped particles become bound again. Already 1000 s after the explosion most of the internal energy deposited by the impact has been converted into

kinetic energy (see Figure 9).

4.2. Hole in the Ejecta

The SN impact affects not only the companion star, but also the SN ejecta themselves. He-rich material is stripped off from the companion due to the SN impact and largely confined to the downstream region behind the companion star, creating a hole in the SN ejecta with an opening angle of $\sim 35^\circ$ with respect to the $x-$axis in our simulation (see Figure 5 and Figure 10a). Recent hydrodynamic simulations suggest that the cone-hole that is created during the interaction could remain for hundreds of years (García-Senz et al. 2012). Kasen et al. (2004) explored the effect of a hole in the SN ejecta on spectra and light curves, suggesting that the cone-hole might be a source of polarization of SN Ia spectra. For a recent review of spectropolarimetry measurements of SNe Ia see Wang & Wheeler (2008).

After the impact, stripped He-rich material is mixed with the SN ejecta (see Figure 11). More SN ejecta material is found to be mixed into the He-filled hole if the orbital motion and spin of the He companion star are considered. The post-impact velocity distributions of the stripped companion material are shown in Figure 10b. The peak velocity of $\sim 800\,\mathrm{km\,s^{-1}}$ moves rightwards to $\sim 1000\,\mathrm{km\,s^{-1}}$ when the orbital and spin velocities of the companion star are included. However, this peak velocity is still smaller than the typical ejecta velocity of $\sim 10^4\,\mathrm{km\,s^{-1}}$, which indicates that the stripped He-rich material is largely hidden in the SN ejecta. It might be possible to detect it in late-time spectra of the SN when the ejecta become transparent (see also Pan et al. 2012). The high excitation energy of He, however, may prevent the formation of He lines in the nebular spectra.

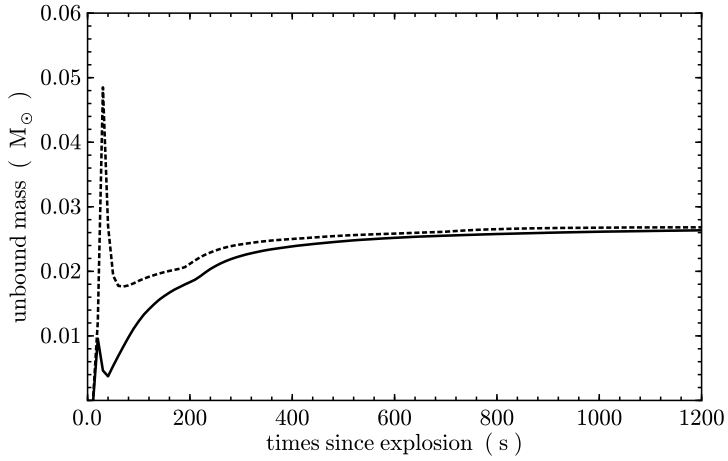

Fig. 9.— Unbound mass vs. simulation time in impact simulations with W7_He01 model. The solid line shows the total mass of all particles with a total energy (kinetic plus potential energy) larger than zero. The dashed line also includes the internal energy in the sum.

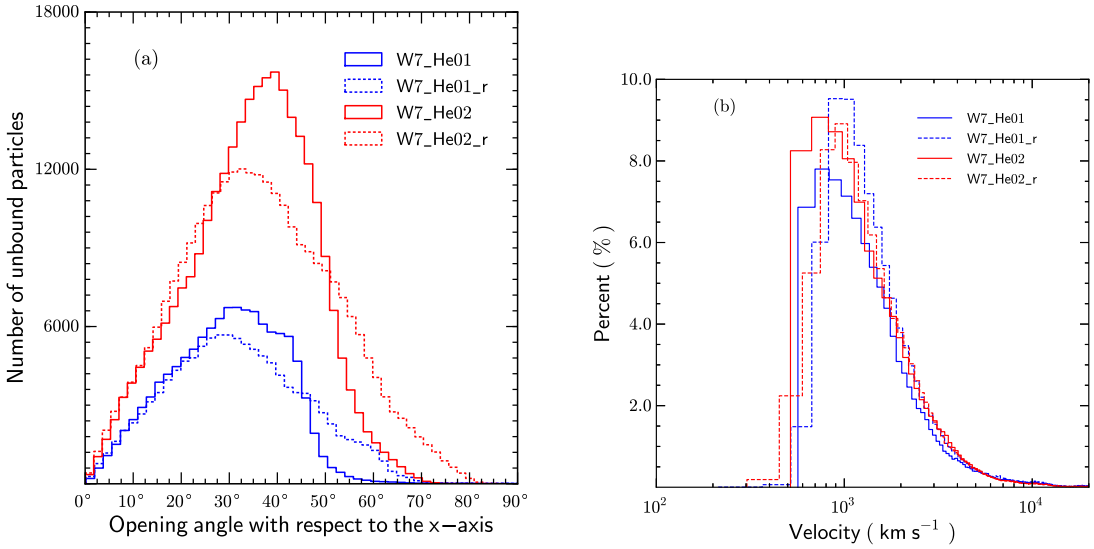

Fig. 10.— *Panel (a)*: distribution of opening angle of all unbound companion particles with respect to the $x-$axis at the end of the simulation. *Panel (b)*: velocity distribution of unbound companion material.

4.3. Accumulation of Ejecta on the Companion Star

4.3.1. Initial velocities of accreted SN ejecta

The envelope of the companion star may be enriched by heavy elements of the SN Ia ejecta while its He-rich material is stripped off by the SN impact. As a consequence a surviving companion star may show unusual chemical signatures if a significant amount of SN ejecta material is accumulated onto the donor star. González Hernández et al. (2009) concluded that Tycho G has an unusually high nickel abundance, and they claimed that it can be explained by the accumulation of SN ejecta. However, the measured [Ni/Fe] ratio from a more recent study of Kerzendorf et al. (2012) seems to be not unusual with respect to field stars with the same metallicity. Unusual abundances become a potential approach to identify the He companion stars in SNRs after the nickel radioactively decays.

In the hydrodynamics simulations, we trace all bound particles that originally belonged to the SN ejecta after the explosion. Figure 12 illustrates the temporal evolution of the amount of bound ejecta in the W7_He01 and W7_He02 models. After the SN explosion, it takes some time for the ejecta material to settle onto the surface of the companion star. Early after the SN explosion, most of the bound ejecta material is found at regions close to the SN explosion center. About $600 - 700\,\mathrm{s}$ after the impact, almost all bound ejecta particles fall onto the companion (see figure 12) and mix with the outer layers of the star. At the end of the simulations ($\sim$2000 s), the total amount of accreted SN ejecta is $M_{\mathrm{tot}}\sim3\text{–}5\times10^{-3}\,\mathrm{M}_{\odot}$ ($M_{\mathrm{Ni}}\sim0.8\text{–}1.6\times10^{-3}\,\mathrm{M}_{\odot}$ and $M_{\mathrm{Fe}}\sim2\text{–}4\times10^{-3}\,\mathrm{M}_{\odot}$) for the W7_He01 and W7_He02 models. The bound nickel mass is similar to the results of the hydrodynamics simulations of Pan et al. (2012). In order to check whether some bound ejecta particles become unbound again at late times, we keep running the W7_He01 and W7_He02 models until 7000 s after the impact. It is found that some bound ejecta particles leave the companion star again, however, the change is only 1%–3%. Therefore, we run all other

simulations in this work to only 2000–3000 s to save computational resources.

Figure 13 shows the abundances of various chemical elements accumulated from the SN ejecta onto the surface of the He companion star at the end of the simulations. Iron-peak elements (especially Fe and Ni) dominate the accreted ejecta (see the vertical gray color range of Figure 13). Note that the masses of unstable isotopes, such as ^{56}Ni, ^{57}Ni and ^{56}Co are also included when summing up the Ni and Co masses. In order to check the original expansion velocity distribution of all accreted ejecta particles, we trace the original positions of all bound ejecta particles in the W7 model (t = 10 s) based on their SPH ID number. The result is shown in Figure 14a. Most of the contamination is attributed to particles with low expansion velocity in the SN ejecta (i.e., the innermost region of the W7 model). The typical peak expansion velocity of accreted ejecta material is $\sim 10^3\,\mathrm{km\,s^{-1}}$. This result can be explained by the lower kinetic energy of those particles which makes it easier to stay at the surface of the companion star after the momentum transfer. The distribution of initial expansion velocities of all accreted iron-peak elements (Cr, Mn, Fe, Co and Ni, which corresponds to the vertical gray range of Figure 13) is further shown in Figure 14b. Again, most accreted iron-peak elements come from the low-velocity tail of the SN ejecta. Therefore, we argue that the composition of the ejecta material that pollutes the companion star is very sensitive to the nuclear burning at the center of the explosion and could, if detected, possibly be used as a diagnostic of the explosion mechanism.

4.3.2. Influence of orbital separation

We checked the sensitivity of the level of total contamination with the orbital separation for a given companion model. The orbital separation is adjusted to cover the range of the A/R_2 parameter suggested by population synthesis calculations as shown in Figure 8a. Figure 15 illustrates how the contamination depends on the orbital separation in the

W7_He01 and W7_He02 models. The amount of SN Ia ejecta deposited on the surface of the He companion star is seen to vary with the orbital separation for a fixed companion model. Larger orbital separation leads to a lower ram pressure and also a smaller cross section, reducing the contamination from SN Ia ejecta. Note, however, that the changes in the orbital separation of the W7_He01 or W7_He02 model are purely artificial. Therefore, the effect of the nature of the He companion star is ignored. The different amount of contamination between W7_He01 and W7_He02 indicates that the details of the companion structure are also important.

Moreover, the comparison between the results of the W7_He01 (or W7_He02) and W7_He01_r (or W7_He02_r) models shows that the asymmetry due to the orbital motion and spin of the He companion star does not significantly affect the amount of the contamination of SN ejecta in our hydrodynamical simulations (see Table 1).

4.3.3. Influence of the Explosion Energy

A 1D parametrized pure deflagration of a $M_{\rm Ch}$ CO WD with a kinetic energy of 1.23×10^{51} erg (i.e., the W7 model, see Nomoto et al. 1984) is used to represent the SN Ia explosion in our hydrodynamics simulations. However, different deflagration and detonation cases cover a typical range of kinetic energies of 0.8–1.6$\times 10^{51}$ erg (Röpke et al. 2007; Gamezo et al. 2005; Seitenzahl et al. 2013). Here, we study how different explosion energies affect the interaction with the companion star.

For this purpose, we use the same method as Pakmor et al. (2008) to artificially adjust the kinetic energy of the SN ejecta $E^i_{\rm kin,SN}$ by scaling the velocities v^i of the SN particles based on the original W7 model (see also Pakmor et al. 2008):

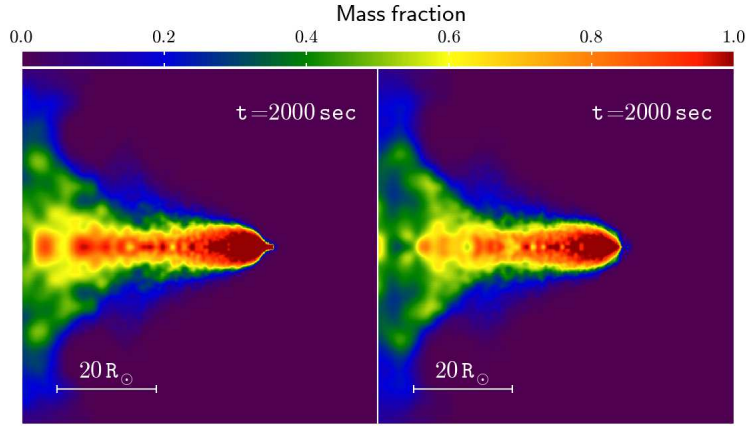

Fig. 11.— Mass fraction of companion material to the SN ejecta in the hydrodynamics simulations of W7_He01 (*left panel*) and W7_He01_r model (*right panel*). The blue end of the color table corresponds to pure SN ejecta material while a the red end of the color table represents pure companion material.

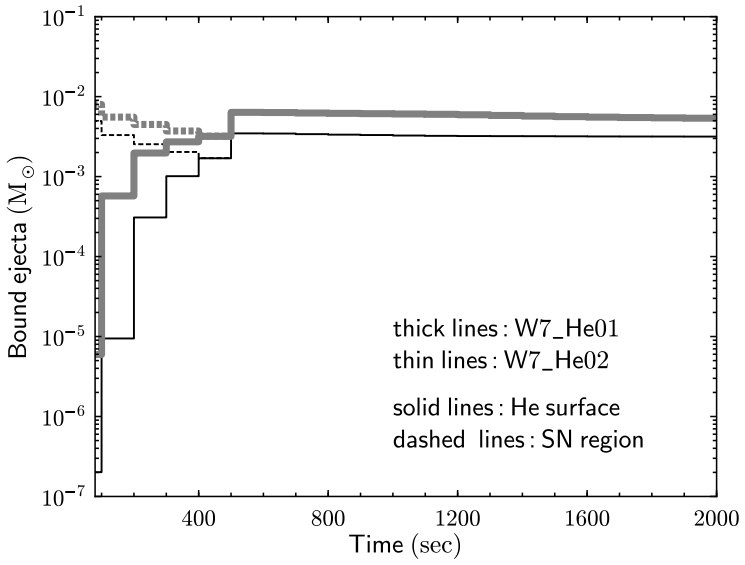

Fig. 12.— Temporal evolution of bound ejecta masses. Early in the SN explosion, most of bound ejecta are found at the regions close to the SN explosion center.

$$v^i = \sqrt{\frac{E^i_{\rm kin,SN}}{E^{\rm W7}_{\rm kin,SN}}} v^{\rm W7}, \tag{5}$$

where $E^{W7}_{\rm kin,SN}$ and $v^{\rm W7}$ are the kinetic energy (1.23×10^{51} erg) and homologous expansion velocity of the ejecta (which corresponds to velocities of expanding shells of SN ejecta) of the original W7 explosion model. This scaling preserves the homologous expansion ($v \propto r$) of the ejecta. Four additional W7-based models with different kinetic energies ($E^i_{\rm kin,SN} = 0.8, 1.0, 1.4$, and 1.6×10^{51} erg) are studied. The lowest of these kinetic energies is consistent with simulations of pure deflagrations in CO WDs (e.g., Röpke et al. 2007). The upper limit is calculated by assuming that a $M_{\rm Ch}$ WD consisting of an equal-by-mass mixture of carbon and oxygen burns completely to ^{56}Ni.

Using the "He01_r" model as a representative case, we investigate the influence of the SN explosion energy on the stripped companion mass, kick velocity and deposited ejecta mass. Numerical results for all W7-based models are shown in Table 1. The stripped mass increases linearly with SN explosion energy (see Figure 16a). With a typical range of explosion energies of 0.8–1.6×10^{51} erg, the stripped companion mass by the SN impact changes by a factor of two. This is consistent with the study of Pakmor et al. (2008) for MS companion stars. Moreover, the dependence of kick velocity and captured ejecta mass on the explosion energy can be fitted with a power law in good approximation (see Figure 16b and Figure 16c). It is not surprising to find that the total contamination increases with decreasing explosion energy. For smaller explosion energies, smaller fractions of the ejecta are able to overcome the gravitational potential energy at the end of momentum exchange. Therefore, a high contamination of $\sim 1.2 \times 10^{-2}\,{\rm M}_\odot$ is found in impact simulations with the lowest explosion energy of 0.8×10^{51} erg (W708_He01_r model, see Table 1).

4.3.4. Decay of unstable isotopes

At the end of our simulations, the envelope of the surviving companion star is enriched by the heavy elements accreted from the low-expansion-velocity tail of the SN ejecta. In order to investigate whether the surviving companion stars would be expected to show observational over-abundance signatures, we estimate the ratio of the bound Ni (or Fe) mass to the envelope He mass of a surviving companion (see Table 1) adopting the method of Pan et al. (2010). We also assume uniform mixing of the contaminants in the envelope. With two different companion models, the ratio of accreted Ni mass to the companion envelope He mass, $M_{\rm Ni}/M_{\rm He}$, is $\sim$2–4$\times10^{-3}$, which corresponds to a value of $(M_{\rm Ni}/M_{\rm He})/(M_{\rm Ni}/M_{\rm H+He})_{\odot}$ $\approx$24–48. At the same time $M_{\rm Fe}/M_{\rm He}\sim$4–9$\times10^{-3}$, which corresponds to $(M_{\rm Fe}/M_{\rm He})/(M_{\rm Fe}/M_{\rm H+He})_{\odot}$ $\approx$2–6. Here, we use the solar composition of Lodders (2003) to obtain the corresponding value of $(M_{\rm Ni}/M_{\rm H+He})_{\odot}$ to compare with our simulation values.

However, the above results neglect the radioactive decay of unstable isotopes. Figure 17 shows that the captured SN ejecta material contains several unstable isotopes (^{56}Ni, ^{56}Co, ^{57}Co, ^{55}Fe, etc), although stable species are the primary components. The further decay of unstable isotopes changes the long timescale Fe (or Ni) abundances of the star. However, compared with the solar value of iron/nickel-to-hydrogen plus helium of Lodders (2003), our simulation values after the radioactive decays are still larger (see Figure 13), providing a possible way to identify a surviving companion star in SNRs by detecting its unusual chemical abundance. We note that our previous hydrodynamical simulations for WD+MS-like models showed that the amount of contamination of SN ejecta is $\lesssim 10^{-5}\,M_{\odot}$ (which corresponds to a small number of ejecta particles). However, this contamination of $\lesssim 10^{-5}\,M_{\odot}$ is too small to ensure whether it is a real contamination or not.

4.3.5. Delayed detonation explosion model

Our hydrodynamics simulations with a classical W7 model show that a surviving companion star in the WD+HE scenario can be significantly enriched by heavy elements of the innermost SN ejecta. However, the precise explosion mechanism of SNe Ia remains unclear. Different composition structures in various SN Ia explosion models might affect the abundance of captured heavy elements after the SN explosion.

To simply predict the effects of different explosion models, mass distributions of ejecta elements of a delayed detonation model (Seitenzahl et al. 2013) after radioactive decays of unstable isotopes are compared with those of the W7 model. Here, we use the 'N100 model' of Seitenzahl et al. (2013) to as an example realization of the delayed detonation mechanism of an SN Ia (see also Röpke et al. 2012. The detailed comparisons within different SN ejecta velocities are shown in Figure 18 and Figure 19. The delayed detonation mechanism in the SD scenario has been suggested to be the most promising way of producing observables in reasonable agreement with observations of normal SNe Ia (Khokhlov 1991). In Section 4.3, it is found that most of the captured heavy elements come from the innermost SN ejecta (see Figure 14). Therefore, we restrict the detailed comparisons in Figure 18 and Figure 19 to SN ejecta regions with an expansion velocity of $\lesssim 5000\,\mathrm{km\,s^{-1}}$.

In Figure 18, the inner ejecta of the 'N100 model' show distinctly smaller masses of stable Ni, Co, Mn and Cr compared to those of the 'W7 model', but basically similar stable Fe mass. Therefore, we can roughly expect that a surviving companion star may be less enhanced with Ni, Co, Mn and Cr due to the relatively ineffective enrichment if we use the N100 model instead of the W7 model to carry out the same impact hydrodynamics simulations. However, we do not expect the N100 model will lead to a surviving companion star with significantly different Fe abundance compared to a surviving companion impacted by W7 ejecta. Moreover, a significant amount of stable Si, Ca, S and Ar within $5000\,\mathrm{km\,s^{-1}}$

in the N100 model indicates that its surviving companion star might show observable signature of Si, Ca, S and Ar enhancement (see Figure 18).

4.4. Indicators of a surviving companion star

In case some SNe Ia originate from the WD+HE $M_{\rm Ch}$ scenario, our simulations indicate that surviving companion stars would show characteristic observational features due to contamination by SN ejecta (see Section 4.3). This may help to identify a surviving companion star even a long time after the SN explosion.

In our simulations, it is found that the kick velocity received by a companion is $\sim$58–67 $\rm km\,s^{-1}$. WMCH09 showed that the He companion has an orbital velocity of $\sim$300–500 $\rm km\,s^{-1}$ at the moment of the SN explosion. This indicates a surviving companion star will have a high spatial velocity that is similar to its pre-explosion orbital velocity.

A small stripped mass ($\sim$0.03–0.06 $\rm M_\odot$) is insufficient to remove the total angular momentum of a He companion (only 13%–38% of initial angular momentum are lost from the star, see Figure 20). Therefore, we expect that He survivors would be rapid rotators (for a detailed discussions of post-impact rotation of surviving companion stars, see Liu et al. 2013; Pan et al. 2013). In WMCH09, it was shown that the pre-explosion rotational velocities of companion stars in the WD+HE $M_{\rm Ch}$ channel are 120–380 $\rm km\,s^{-1}$ assuming that the rotation of the companion star is phase-locked to its orbital motion due to tidal forces.

At the end of our simulations, about 0.028–0.056 $\rm M_\odot$ of He-rich material are stripped off from the He companion stars. Full radiative transport calculations with the results of our hydrodynamics simulations are required to assess the possibility of detecting He lines in the nebular spectra of the modeled events.

After the SN impact, a surviving companion star dramatically puffs up due to the significant SN heating, and it would become a luminous He star near the SNR center while its equilibrium is reestablished during several centuries after the explosion (Pan et al. 2013). Moreover, it may be a rapidly rotating star with a high spatial velocity (see Pan et al. 2013).

One way to verify the WD+HE progenitor scenario is by identifying a corresponding surviving star in a SN remnant.

5. SUMMARY AND CONCLUSIONS

The primary goal of this work has been to investigate the interaction of SN Ia ejecta with the companion star within the WD+HE $M_{\rm Ch}$ explosion scenario. We mainly focused on whether or not a surviving companion shows an unusual abundance signature after the SN explosion. We have performed 3D hydrodynamics impact simulations employing the SPH code Stellar GADGET. The effect of the orbital motion and spin of the companion star were also taken into account. Two representative He companion models were obtained from 1D consistent binary evolution calculations with Eggleton's stellar evolution code, treating the mass loss of the donor star as RLOF. Our main conclusions are summarized as follows:

- In the WD+HE $M_{\rm Ch}$ scenario, it is found that only ∼2%–5% of the initial companion mass can be stripped off due to the SN impact. The star receives a small kick velocity of ∼58–67 $\rm km\,s^{-1}$.
- A power-law relation similar to that of (Pan et al. 2010, 2012) is found between the unbound mass (or kick velocity) and the orbital separation for a given companion star model.

- The orbital motion and spin of a He companion star do not significantly affect the amount of unbound mass and kick velocity caused by the SN impact.
- Our simulations predict that a surviving companion star in the WD+HE $M_{\rm Ch}$ channel moves with a high spatial velocity and should be a fast rotator after the SN explosion.
- The He companion star is enriched by the heavy elements with low expansion velocity of the SN Ia ejecta. The total contamination is $\gtrsim 10^{-3}\,{\rm M}_{\odot}$, providing a potential way to identify a survivor after the SN explosion.
- The amount of contamination from SN Ia ejecta decreases with the increase of SN explosion energy and can be fitted with a power-law relation in good approximation.

Our results are based on the standard SN Ia explosion model 'W7' (Nomoto et al. 1984; Maeda et al. 2010). The comparison in Section 4.3.5 indicates that more comprehensive investigations with various state-of-the-art explosion models are needed to reliably predict whether the surviving companion star in the WD+HE $M_{\rm Ch}$ channel would show unusual abundances.

Acknowledgments

We thank U. Noebauer for very useful discussions. Z.W.L and Z.W.H thank the financial support from the MPG-CAS Joint Doctoral Promotion Program (DPP) and Max Planck Institute for Astrophysics (MPA). This work is supported by the National Basic Research Program of China (Grant No. 2009CB824800), the National Natural Science Foundation of China (Grant Nos. 11033008 and 11103072) and the Chinese Academy of Sciences (Grant N0. KJCX2-YW-T24). The work of F.K.R was supported by Deutsche Forschungsgemeinschaft (DFG) via the Emmy Noether Program (RO 3676/1-1) and by the

ARCHES prize of the German Federal Ministry of Education and Research (BMBF). The work by K.M. is supported by World Premier International Research Center Initiative (WPI Initiative), MEXT, Japan, and by Grant-in-Aid for Scientific Research for Young Scientists (23740141). S.T. is supported by the DFG through the Transregional Collaborative Research Centre 'The Dark Universe' (TRR 33). The simulations were carried out at the Computing Center of the Max Planck Society, Garching, Germany.

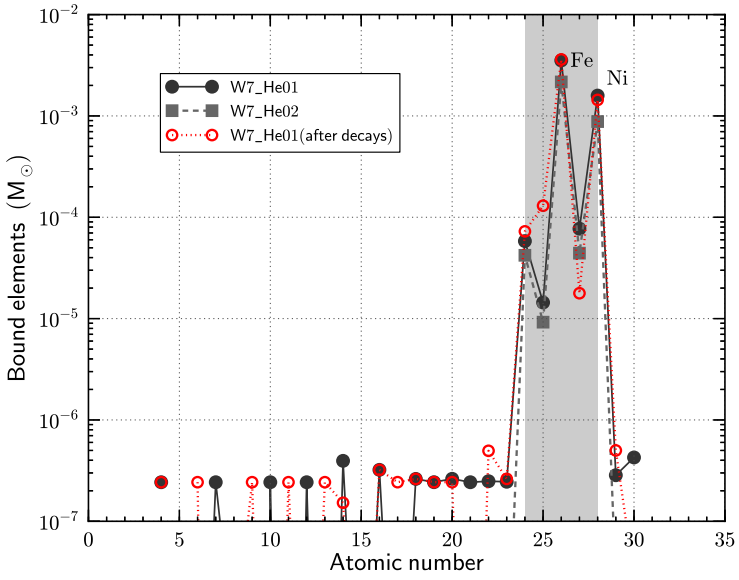

Fig. 13.— Chemical composition of the accreted ejecta material ∼2000 s after the explosion for the W7_He01 and W7_He02 models. The corresponding composition of the accreted ejecta after decays of unstable isotopes for W7_He01 model is shown with open circles.

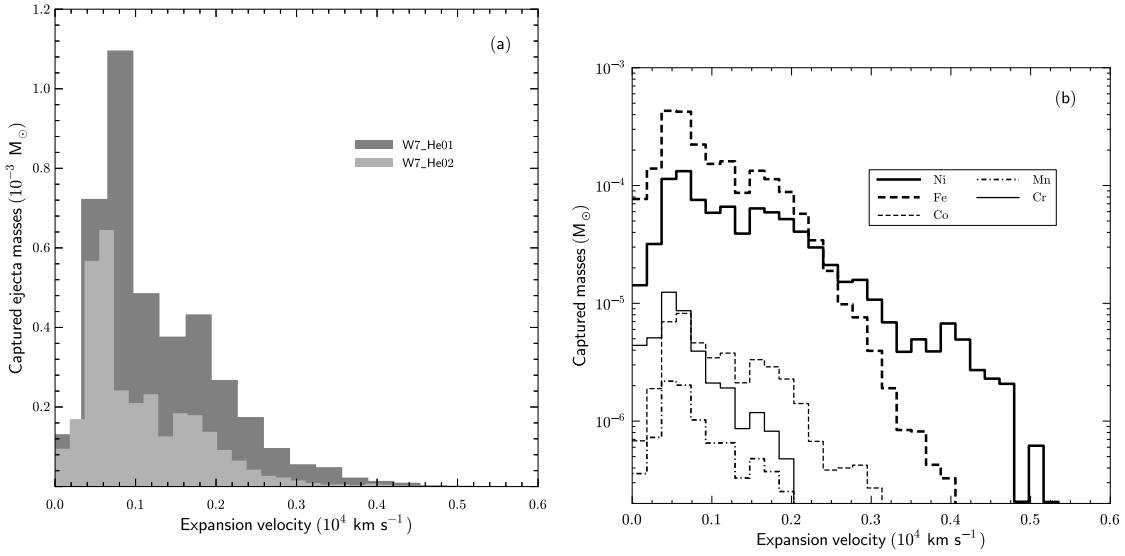

Fig. 14.— *Panel (a)*: distribution of bound ejecta in their initial expansion velocity space (at 10 s after the explosion). *Panel (b)*: similar to *Panel (a)*, but only includes the iron-peak elements of the W7_He02 model (Cr, Mn, Fe, Co and Ni) which correspond to the vertical gray range of Figure 13.

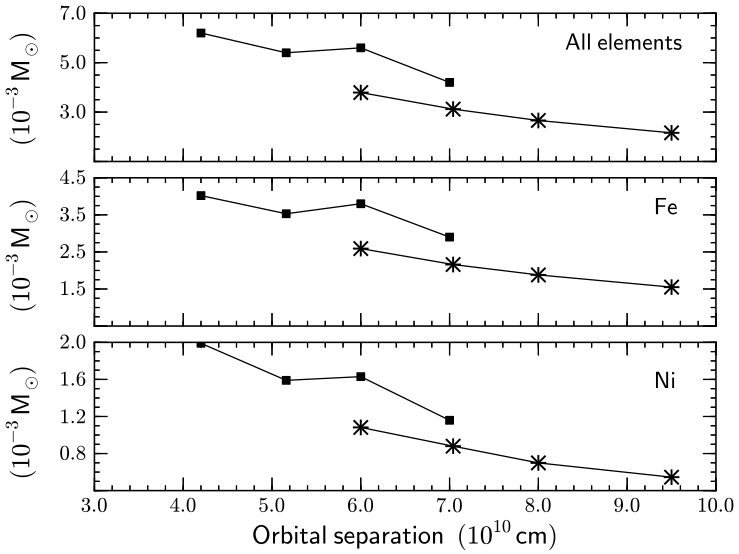

Fig. 15.— Dependence of bound-ejecta mass on the orbital separation in impact simulations with W7_He01 (*square markers*) and W7_He02 model (*star markers*). All values are measured at the end of the SPH impact simulations.

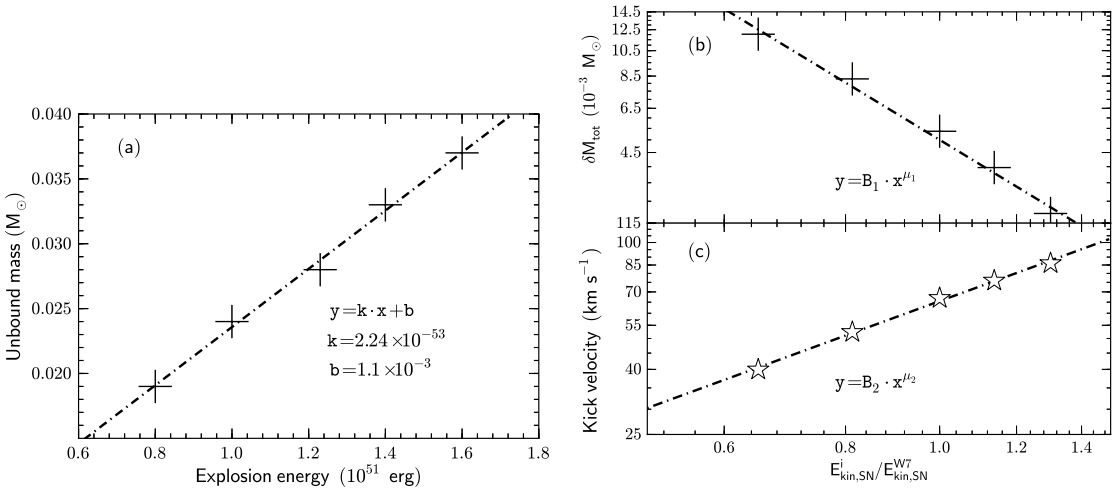

Fig. 16.— *Panel (a)*: Total stripped mass as a function of the SN explosion energy (see Table 1). *Panel (b)*: Power-law fit of the dependence of total accreted ejecta masses ($B_1 = 0.005$, $\mu_1 = -2.133$) on the SN explosion energy (Table 1). *Panel (c)*: Similar as *Panel (b)*, but for the kick velocity ($B_2 = 65.49$, $\mu_2 = 1.114$). The star and corss symbols represent the results of the impact simulations. Lines show fitted linear (power-law) relations based on the numerical simulation results.

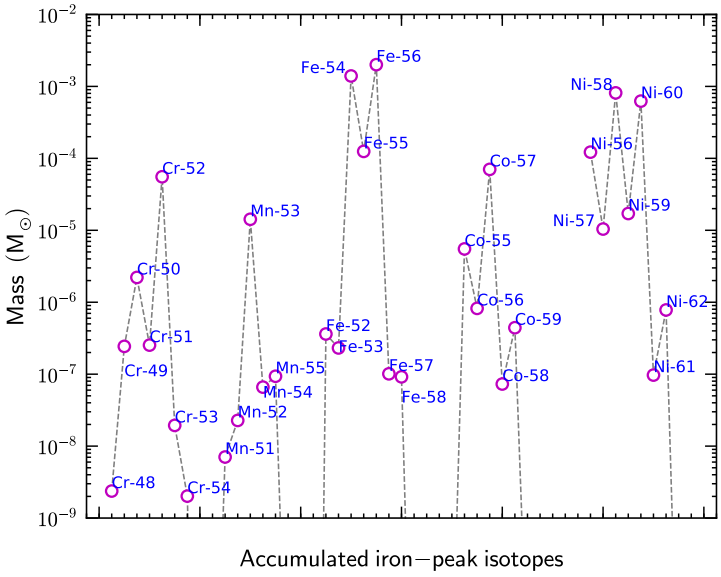

Fig. 17.— Details of mass distributions of stable and unstable isotopes of accreted iron-peak elements (Cr, Mn, Fe, Co and Ni, i.e., vertical gray range of Figure 13) in the impact simulations for W7_He01 model.

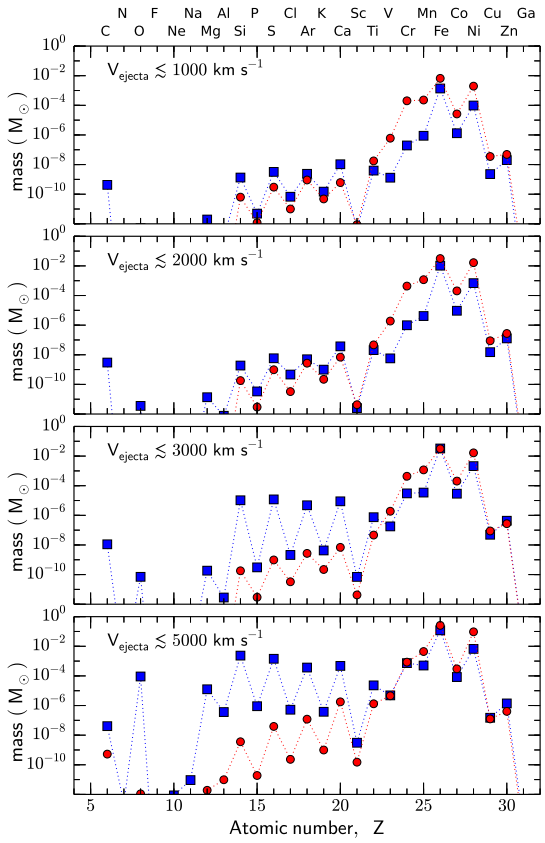

Fig. 18.— Chemical composition of a delayed detonation model of 'N100' (*squares*) (Seitenzahl et al. 2013) and the W7 model (*circles*) after radioactive decays of unstable isotopes. Different panels show details of the composition for different ejecta regions of the inner $1000, 2000, 3000, 5000\,\mathrm{km\,s^{-1}}$. For example, the top (or bottom) panel shows the chemical composition of all ejecta material inside the spherical shell at ejecta velocity of $1000\,\mathrm{km\,s^{-1}}$ (or $5000\,\mathrm{km\,s^{-1}}$).

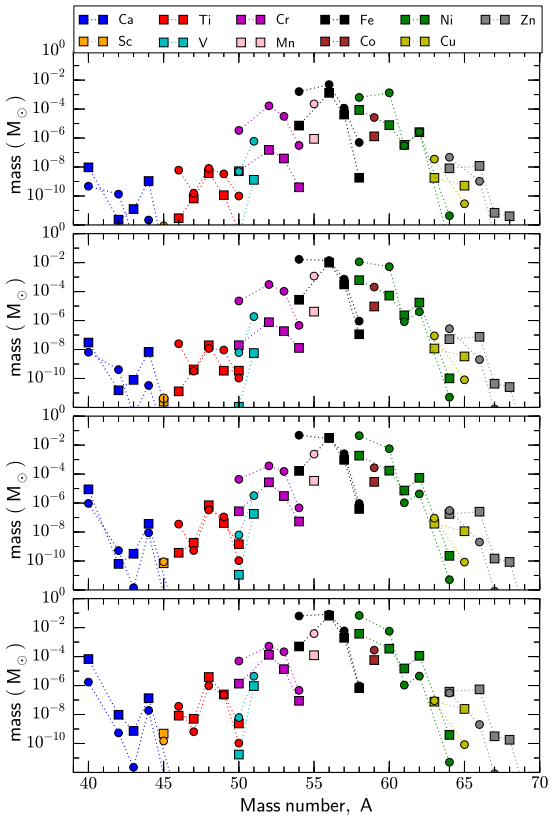

Fig. 19.— Similar to Figure 18, but for different isotopes of selected elements from Ca to Zn. Squares are the delayed detonation model (i.e., N100 model) and circles are the W7 model.

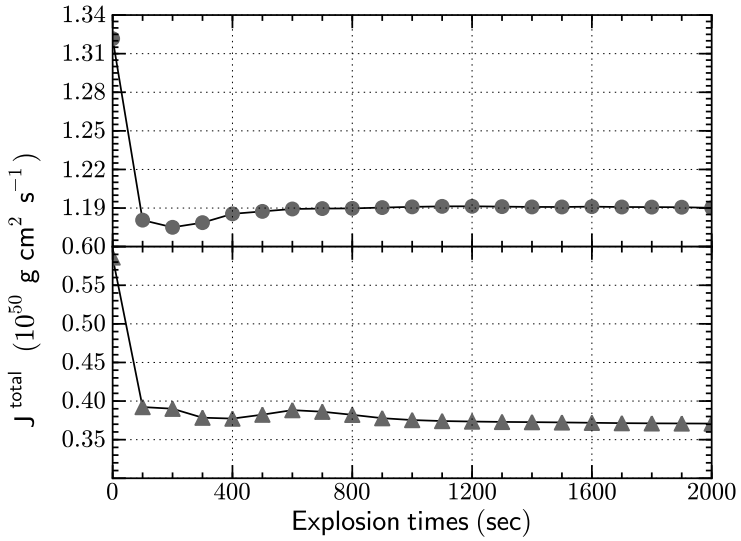

Fig. 20.— Temporal evolution of the total angular momentum of the companion star in W7_He01_r (*top panel*) and W7_He02_r (*bottom panel*) model (see Table 1).

REFERENCES

Bloom, J. S., Kasen, D., Shen, K. J., et al. 2012, ApJ, 744, L17

Chomiuk, L., Soderberg, A. M., Moe, M., et al. 2012, ApJ, 750, 164

Dewi, J. D. M., Pols, O. R., Savonije, G. J., & van den Heuvel, E. P. J. 2002, MNRAS, 331, 1027

Di Stefano, R., & Kilic, M. 2012, ApJ, 759, 56

Di Stefano, R., Voss, R., & Claeys, J. S. W. 2011, ApJ, 738, L1

Dilday, B., Howell, D. A., Cenko, S. B., et al. 2012, Science, 337, 942

Eggleton, P. P. 1971, MNRAS, 151, 351

—. 1972, MNRAS, 156, 361

—. 1973, MNRAS, 163, 279

—. 1983, ApJ, 268, 368

Fink, M., Hillebrandt, W., & Röpke, F. K. 2007, A&A, 476, 1133

Fink, M., Röpke, F. K., Hillebrandt, W., et al. 2010, A&A, 514, A53

Foley, R. J., Kromer, M., Howie Marion, G., et al. 2012, ApJ, 753, L5

Gamezo, V. N., Khokhlov, A. M., & Oran, E. S. 2005, ApJ, 623, 337

García-Senz, D., Badenes, C., & Serichol, N. 2012, ApJ, 745, 75

González Hernández, J. I., Ruiz-Lapuente, P., Filippenko, A. V., et al. 2009, ApJ, 691, 1

Hachisu, I., Kato, M., & Nomoto, K. 1996, ApJ, 470, L97

—. 1999, ApJ, 522, 487

Han, Z., & Podsiadlowski, P. 2004, MNRAS, 350, 1301

Hillebrandt, W., Kromer, M., Röpke, F. K., & Ruiter, A. J. 2013, ArXiv e-prints

Hillebrandt, W., & Niemeyer, J. C. 2000, ARA&A, 38, 191

Horesh, A., Kulkarni, S. R., Fox, D. B., et al. 2012, ApJ, 746, 21

Iben, Jr., I., & Tutukov, A. V. 1984, ApJS, 54, 335

Justham, S. 2011, ApJ, 730, L34

Kasen, D., Nugent, P., Thomas, R. C., & Wang, L. 2004, ApJ, 610, 876

Kato, M., & Hachisu, I. 2004, ApJ, 613, L129

Kerzendorf, W. E., Yong, D., Schmidt, B. P., et al. 2012, ArXiv e-prints

Khokhlov, A. M. 1991, A&A, 245, 114

Landau, L. D., & Lifshitz, E. M. 1971, The classical theory of fields

Lentz, E. J., Baron, E., Branch, D., & Hauschildt, P. H. 2001, ApJ, 557, 266

Leonard, D. C. 2007, ApJ, 670, 1275

Li, W., Bloom, J. S., Podsiadlowski, P., et al. 2011, Nature, 480, 348

Liu, Z.-W., Pakmor, R., Roepke, F. K., et al. 2013, ArXiv:1303.2691

Liu, Z. W., Pakmor, R., Röpke, F. K., et al. 2012, A&A, 548, A2

Lodders, K. 2003, ApJ, 591, 1220

Maeda, K., Benetti, S., Stritzinger, M., et al. 2010, Nature, 466, 82

Maoz, D., & Badenes, C. 2010, MNRAS, 407, 1314

Maoz, D., & Mannucci, F. 2012, PASA, 29, 447

Maoz, D., Sharon, K., & Gal-Yam, A. 2010, ApJ, 722, 1879

Marietta, E., Burrows, A., & Fryxell, B. 2000, ApJS, 128, 615

Nomoto, K. 1982, ApJ, 253, 798

Nomoto, K., & Iben, Jr., I. 1985, ApJ, 297, 531

Nomoto, K., Saio, H., Kato, M., & Hachisu, I. 2007, ApJ, 663, 1269

Nomoto, K., Thielemann, F.-K., & Yokoi, K. 1984, ApJ, 286, 644

Nugent, P. E., Sullivan, M., Cenko, S. B., et al. 2011, Nature, 480, 344

Pakmor, R., Edelmann, P., Röpke, F. K., & Hillebrandt, W. 2012a, MNRAS, 424, 2222

Pakmor, R., Hachinger, S., Röpke, F. K., & Hillebrandt, W. 2011, A&A, 528, A117

Pakmor, R., Kromer, M., Röpke, F. K., et al. 2010, Nature, 463, 61

Pakmor, R., Kromer, M., & Taubenberger, S. 2013, ArXiv:1302.2913

Pakmor, R., Kromer, M., Taubenberger, S., et al. 2012b, ApJ, 747, L10

Pakmor, R., Röpke, F. K., Weiss, A., & Hillebrandt, W. 2008, A&A, 489, 943

Pan, K.-C., Ricker, P., & Taam, R. 2013, ArXiv:1303.1228

Pan, K.-C., Ricker, P. M., & Taam, R. E. 2010, ApJ, 715, 78

—. 2012, ApJ, 750, 151

Patat, F., Chandra, P., Chevalier, R., et al. 2007, Science, 317, 924

Perlmutter, S., Aldering, G., Goldhaber, G., et al. 1999, ApJ, 517, 565

Price, D. J. 2007, PASA, 24, 159

Riess, A. G., Filippenko, A. V., Challis, P., et al. 1998, AJ, 116, 1009

Röpke, F. K., Hillebrandt, W., Schmidt, W., et al. 2007, ApJ, 668, 1132

Röpke, F. K., Kromer, M., Seitenzahl, I. R., et al. 2012, ApJ, 750, L19

Ruiter, A. J., Belczynski, K., & Fryer, C. 2009, ApJ, 699, 2026

Schaefer, B. E., & Pagnotta, A. 2012, Nature, 481, 164

Schmidt, B. P., Suntzeff, N. B., Phillips, M. M., et al. 1998, ApJ, 507, 46

Seitenzahl, I. R., Ciaraldi-Schoolmann, F., Röpke, F. K., et al. 2013, MNRAS, 429, 1156

Shappee, B. J., Stanek, K. Z., Pogge, R. W., & Garnavich, P. M. 2013, ApJ, 762, L5

Shen, K. J., Guillochon, J., & Foley, R. J. 2013, ArXiv e-prints

Springel, V. 2005, MNRAS, 364, 1105

Sternberg, A., Gal-Yam, A., Simon, J. D., et al. 2011, Science, 333, 856

Timmes, F. X., Woosley, S. E., & Taam, R. E. 1994, ApJ, 420, 348

Wang, B., Chen, X., Meng, X., & Han, Z. 2009a, ApJ, 701, 1540

Wang, B., & Han, Z. 2010, A&A, 515, A88

Wang, B., Li, X.-D., & Han, Z.-W. 2010, MNRAS, 401, 2729

Wang, B., Meng, X., Chen, X., & Han, Z. 2009b, MNRAS, 395, 847

Wang, L., & Wheeler, J. C. 2008, ARA&A, 46, 433

Webbink, R. F. 1984, ApJ, 277, 355

Whelan, J., & Iben, Jr., I. 1973, ApJ, 186, 1007

Woosley, S. E., & Kasen, D. 2011, ApJ, 734, 38

Woosley, S. E., Taam, R. E., & Weaver, T. A. 1986, ApJ, 301, 601

Woosley, S. E., & Weaver, T. A. 1994, ApJ, 423, 371